Publication Year	2015
Acceptance in OA@INAF	2020-03-23T15:50:38Z
Title	On the Distance of the Globular Cluster M4 (NGC 6121) Using RR Lyrae Stars. II. Mid-infrared Period-luminosity Relations
Authors	Neeley, J. R.; Marengo, M.; Bono, G.; Braga, Vittorio Francesco; DALL'ORA, Massimo; et al.
DOI	10.1088/0004-637X/808/1/11
Handle	http://hdl.handle.net/20.500.12386/23468
Journal	THE ASTROPHYSICAL JOURNAL
Number	808

The Astrophysical Journal, 808:11 (15pp), 2015 July 20 doi:10.1088/0004-637X/808/1/11
© 2015. The American Astronomical Society. All rights reserved.

ON THE DISTANCE OF THE GLOBULAR CLUSTER M4 (NGC 6121) USING RR LYRAE STARS. II. MID-INFRARED PERIOD–LUMINOSITY RELATIONS

J. R. Neeley[1], M. Marengo[1], G. Bono[2,3], V. F. Braga[2,3], M. Dall'Ora[4], P. B. Stetson[5], R. Buonanno[2,6], I. Ferraro[3], W. L. Freedman[8], G. Iannicola[3], B. F. Madore[9], N. Matsunaga[7], A. Monson[9], S. E. Persson[9], V. Scowcroft[9], and M. Seibert[9]

[1] Department of Physics and Astronomy, Iowa State University, Ames, IA 50011, USA
[2] Department of Physics, Università di Roma Tor Vergara, via della Ricerca Scientifica 1, I-00133 Roma, Italy
[3] INAF-Osservatorio Astronomico di Roma, via Frascati 33, I-00040 Monte Porzio Catone, Italy
[4] INAF-Osservatorio Astronomico di Capodimonte, Salita Moiarello 16, I-80131 Napoli, Italy
[5] NRC-Herzberg, Dominion Astrophysical Observatory, 5071 West Saanich Road, Victoria BC V9E 2E7, Canada
[6] INAF-Osservatorio Astronomico di Teramo, Via Mentore Maggini s.n.c., I-64100 Teramo, Italy
[7] Kiso Observatory, Institute of Astronomy, School of Science, The University of Tokyo, Mitake 10763-30, Kiso-machi, Kiso-gun, 3 Nagano 97-0101, Japan
[8] Department of Astronomy and Astrophysics, University of Chicago, Chicago, IL 60637, USA
[9] Carnegie Observatories, 813 Santa Barbara Street, Pasadena, CA 91101, USA
Received 2015 March 10; accepted 2015 May 27; published 2015 July 14

ABSTRACT

New mid-infrared (MIR) period–luminosity (PL) relations are presented for RR Lyræ variables in the globular cluster M4 (NGC 6121). Accurate photometry was obtained for 37 RR Lyræ variables using observations from the Infrared Array Camera on board the *Spitzer Space Telescope*. The dispersion of M4's PL relations is 0.056, and the uncertainty in the slope is 0.11 mag. Additionally, we established calibrated PL relations at 3.6 and 4.5 μm using published *Hubble Space Telescope* geometric parallaxes of five Galactic RR Lyræ stars. The resulting band-averaged distance modulus for M4 is $\mu = 11.399 \pm 0.007(\mathrm{stat}) \pm 0.080(\mathrm{syst}) \pm 0.015(\mathrm{cal}) \pm 0.020(\mathrm{ext})$. The systematic uncertainty will be greatly reduced when parallaxes of more stars become available from the *GAIA* mission. Optical and infrared period–color (PC) relations are also presented, and the lack of an MIR PC relation suggests that RR Lyræ stars are not affected by CO absorption in the 4.5 μm band.

Key words: globular clusters: individual (M4) – stars: distances – stars: horizontal-branch – stars: variables: RR Lyrae

Supporting material: machine-readable table

1. INTRODUCTION

RR Lyræ variables are important tools in the investigation of many fundamental astrophysical problems. They provide crucial constraints on the physical mechanisms driving radial oscillations and their interplay with stellar evolution (Cox 1963; Christy 1966; Castor 1971). Furthermore, RR Lyræ stars offer the opportunity to study the morphology of the horizontal branch and the Oosterhoff dichotomy (Oosterhoff 1939). Current empirical evidence indicates that the mean period of fundamental mode (RRab or FU) RR Lyræ stars in galactic globular clusters (GGCs hereafter) shows a dichotomous distribution at 0.55 (OoI) and 0.65 (OoII) days (Sandage 1993), where the latter group is more metal-poor. There is also evidence that the dichotomy is the aftermath of the hysteresis mechanism suggested by van Albada & Baker (1973), i.e., that the pulsation mode depends on the direction of the evolution inside the instability strip (Bono et al. 1997; Fiorentino et al. 2012; Kunder et al. 2013). Baade (1944) employed the RR Lyræ stars as a probe to identify the two main stellar populations in the galaxy, as well as to study the stellar content of the galactic bulge through low-reddening regions (Baade 1957; Plaut 1968).

Beyond stellar evolution, RR Lyræ variables have also played a key role in providing estimates of cosmological parameters, and have been instrumental in measuring the distances to a sizable sample of GGcs. This allowed the estimation of absolute cluster ages, and in turn set the lower limit on the age of the universe (Hesser 1991; Sandage 1993; Buonanno et al. 1998; Marín-Franch et al. 2009; Bono et al. 2010; VandenBerg et al. 2013). Moreover, RR Lyræ variables have been used to estimate the primordial helium content using the *A*-parameter, i.e., the mass-to-luminosity relation of low-mass central helium-burning stars (Caputo et al. 1983; Sandquist 2010).

RR Lyræ stars are also the most commonly adopted Population II distance indicators. With a lower mass than classical Cepheids, they have the key advantage of being ubiquitous and have been identified in both early- and late-type stellar systems (van den Bergh 1999). Their individual distances can be evaluated using multiple diagnostics, including a visual magnitude–metallicity relation (Chaboyer et al. 1996; Bono et al. 2003; Cacciari & Clementini 2003) and a statistical parallax (Dambis et al. 2013; Kollmeier et al. 2013). More importantly, they obey to well defined near-infrared (NIR) period–luminosity (PL) relations (Longmore et al. 1986; Bono et al. 2001, 2003; Catelan et al. 2004; Braga et al. 2015). These PL relations extend to mid-infrared (MIR) bands where they have the potential of being very accurate distance indicators due to lower extinction and smaller intrinsic scatter (Madore et al. 2013; Klein et al. 2014). The use of the *I*,V–I reddening free period–Wesenheit (PW) relation to estimate the individual distances of RR Lyræ stars dates back to Soszynski et al. (2003) and to Majaess (2010). A more recent theoretical framework developed by Marconi et al. (2015) further supports the use of optical, optical-NIR, and NIR period–Wesenheit–metallicity relations to determine individual distances of RR Lyræ stars. Empirical validations

to the above pulsation and evolutionary predictions have been provided by Braga et al. (2015) for RR Lyræ stars in the GGC M4 and by G. Coppola et al. (2015, in preparation) for RR Lyræ stars in the Carina dwarf spheroidal.

The Carnegie RR Lyræ Program (CRRP) aims to take full advantage of the unique characteristics of these stars in order to reduce the remaining sources of uncertainty in the Hubble constant to ±2%. RR Lyræ MIR PL relations will be used as the foundation of an independent Population II cosmological distance scale to calibrate TRGB distances for nearby distances, which, in turn, can be used to calibrate SN Ia distances. To achieve this goal, we observed over 1700 RR Lyræ variables in 31 selected GGCs, as well as ∼3000 RR Lyræ stars in strategically distributed areas in the galactic halo and the bulge. In addition, we observed 48 of the nearest, brightest and less reddened RR Lyræ stars intended to be used as zero-point calibrators. These observations have been conducted during the warm mission of the *Spitzer Space Telescope* (Werner et al. 2004) Infrared Array Camera (IRAC, Fazio et al. 2004), at 3.6 and 4.5 μm wavelengths, with a cadence designed to obtain complete coverage of each RR Lyræ variable over at least one full period.

In this work, we focus on the GGC Messier 4 (M4, NGC 6121). This cluster is an ideal laboratory for stellar population studies given its proximity to the Sun, which allows us to obtain accurate photometric and spectroscopic data for member stars well below the main-sequence turnoff. Due to these characteristics, M4 has been the subject of intensive observational campaigns over a wide range of wavelengths. It has a well-characterized differential extinction of $E(B-V) = 0.37 \pm 0.10$ mag, where the uncertainty is the dispersion due to differential reddening (Hendricks et al. 2012) and mean metallicity of [Fe/H] = −1.10 (Braga et al. 2015 and references therein). In support of the CRRP program, we have analyzed available multi-epoch optical and NIR data, leading to the identification and characterization of 45 RR Lyræ variables (Stetson et al. 2014). From these observations, we have derived accurate distance moduli based on optical and NIR PL and PW relations (Braga et al. 2015). In this paper, we combine our previous results with the new MIR data obtained as part of the CRRP campaign.

In Section 2, we present our new *Spitzer* photometry. Light curves for all of the RR Lyræ variables in our sample are measured in Section 3. In Section 4, we derive MIR PL and period–color (PC) relationships for the cluster RR Lyræ variables, while in Section 5 we calculate the M4 distance modulus by calibrating our PL zero point using five nearby calibrator RR Lyræ stars with known parallax, also observed as part of the CRRP program. Dependence of the PL zero point from metallicity is also discussed in Section 5, while Section 6 summarizes the results of this work.

2. OBSERVATIONS, DATA REDUCTION, AND PHOTOMETRY

The results of our ground-based optical and NIR monitoring of the stellar population in M4 have been published in Stetson et al. (2014) and Braga et al. (2015). In this paper, we extend our wavelength coverage to the MIR, by including multi-epoch 3.6 and 4.5 μm photometry of a large portion of the cluster.

Our IRAC observations of M4 were executed on 2013 June 2–3 as part of the warm *Spitzer Space Telescope* Cycle 9 (PID 90088). The cluster was observed at IRAC 3.6 and 4.5 μm bands at 12 equally spaced epochs over ∼14 hr. For each epoch we obtained 30 frames with a medium scale five-point Gaussian dither pattern and a 3 × 2 mapping, taken using the IRAC full frame mode with a frame time of 30 s to provide a median total exposure of 804 s pixel^{-1}. An 11′ × 9′ area at the center of the cluster was covered in both the 3.6 and 4.5 μm bands. Due to the IRAC focal plane array configuration, in the outer regions of the cluster, only one band is available, with the area just north of the center of the cluster only covered at 3.6 μm and the region south of the center only covered at 4.5 μm. The total area mapped by our observations covers a strip of 11′ × 22′, roughly cutting north to south through the center of the cluster, as shown in Figure 1. This is about one-third of the total cluster area that was mapped in our ground-based optical and NIR observations, but is still ∼1.5× the size of the half-mass radius of M4 (3.′65 according to Harris 1996).

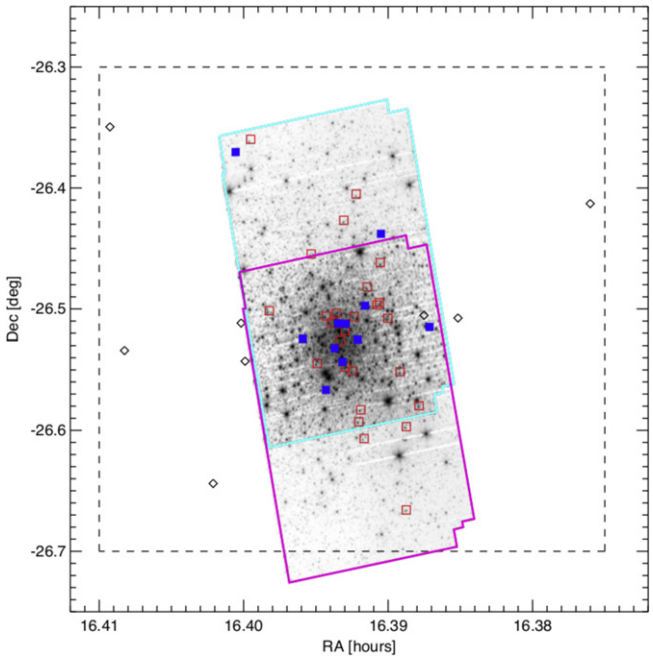

Figure 1. Map of all M4 stars for which we have MIR photometric measurements. The open red and filled blue squares display the position of fundamental and first overtone RR Lyræ stars, respectively. The black diamonds are RR Lyræ from our optical catalog that are not matched in the IRAC catalog. The solid cyan and magenta lines indicate the coverage of the IRAC 3.6 and 4.5 μm data, respectively. The dashed line indicates the approximate field of view of the optical photometry in Stetson et al. (2014). North is up, east is left.

The CRRP IRAC data were reduced starting from the Basic Calibrated Data (BCDs) generated by the *Spitzer* IRAC pipeline version S19.1.0. Photometry was performed using the most recent version of the DAOPHOT/ALLSTAR/ALLFRAME suite of programs for crowded-field stellar photometry (Stetson 1987, 1994). In order to mitigate the effect of blending in the photometry of the M4 crowded field, we used an input source catalog derived by the higher angular resolution optical and NIR images described in Stetson et al. (2014). In addition to higher resolution, this input source catalog is also deeper. For the optical and NIR, accurate photometry was achieved down to 24 and 22 mag, respectively, compared to 17 mag for the MIR images. This catalog was matched to the *Spitzer* data after applying higher order geometric corrections to the individual IRAC BCDs than the

default ones provided by the *Spitzer* IRAC pipeline. With this procedure, we matched 17,595 sources at 3.6 μm and 16,313 sources at 4.5 μm, for which we measured an instrumental magnitude with variable point-spread function (PSF) fitting. The astrometric accuracy of our final source catalog is of the order of 0.″3.

For the optical and NIR images, good photometry was achieved down to 24 and 20 mag, respectively.

The photometry was calibrated to standard IRAC Vega magnitudes using aperture photometry on mosaic images. The mosaics were generated using the IRACproc package (Schuster et al. 2006), a Perl Data Language wrapper script for the standard Spitzer Science Center mosaicking software MOPEX (Makovoz & Khan 2005). We adopted a mosaic pixel scale of 0.″61 pixel^{-1}, or half the native IRAC pixel scale. The stars we selected for the aperture photometry calibration are far from the center of the cluster to reduce blending. In addition, we removed any possible variable stars by avoiding sources with a Welch and Stetson variability index (Welch & Stetson 1993; Stetson 1996) greater than 1σ from the median. We selected a total of 38 stars at 3.6 μm and 44 at 4.5 μm. We used an aperture of three native IRAC pixels ($\simeq$3.″66) with an annulus of 3–7 pixels (3.″66–8.″54). The aperture corrections necessary to convert magnitudes derived with this aperture/annulus combination to the standard IRAC 10 pixels aperture photometry are 1.1284 and 1.1274 for 3.6 and 4.5 μm, respectively, calculated on isolated stars in the mosaics. The calibrating stars cover a range of 4 mag and are distributed randomly across the array, outside of the central region.

Despite the relatively small size of our adopted photometric apertures, the crowding of the field even outside the center of the cluster (M4 is projected behind the Scorpius–Ophiuchus cloud complex) still results in blending contamination of aperture photometry for our calibration sources. These blended sources are, however, in many cases, resolved by the PSF fitting procedure performed in DAOPHOT on the higher resolution visible and NIR images, from which our input catalog is derived. We thus used our point-source photometric catalog to improve the photometric zero point calibration by subtracting from the calibrator aperture photometry the flux (measured from the PSF-fitting photometry) of any blended sources found within our chosen aperture. For each blended source we estimated the contaminating flux by measuring the fraction of its flux falling within our 3 pixels aperture, as a function of its centroid distance from the aperture's center. For this task, we used the IRAC PSF described in Hora et al. (2012), taking advantage of its higher sampling ($\sim$1/100 of the native IRAC pixels) to derive corrections for fractional pixel shifts. At 3.6 μm, 17 of our 38 calibrators were found to be contaminated by an average of 0.03 mag. The 4.5 μm region was less crowded, resulting in only 7 out of 44 contaminated calibrators, but contaminated by 0.11 mag on average.

The magnitudes of the de-blended calibrators were then subtracted from their DAOPHOT instrumental magnitudes to derive the final calibration zero point. We found no trend in the calibration zero point with either brightness or array location. The uncertainty in our final calibration is 0.018 mag at 3.6 μm and 0.017 mag at 4.5 μm, based on the standard deviation between the instrumental and measured magnitudes. This standard deviation of the calibration increases dramatically for the fainter stars in our calibration sample. If we select only calibrating stars brighter than 14 mag, then the error in the calibration is reduced to 0.015 at 3.6 μm and 0.013 at 4.5 μm.

Table 1
Photometry for RR Lyrae in M4

MJD[a]	[3.6] mag	$\sigma_{[3.6]}$	MJD[a]	[4.5] mag	$\sigma_{[4.5]}$
56446.223	11.354	0.030	56446.227	11.267	0.079
56446.285	11.376	0.010	56446.293	11.317	0.050
56446.336	11.394	0.003	56446.340	11.318	0.051
56446.391	11.329	0.011	56446.398	11.261	0.074
56446.438	11.302	0.012	56446.441	11.224	0.089
56446.492	11.312	0.021	56446.496	11.248	0.076
56446.543	11.358	0.016	56446.547	11.285	0.069
56446.598	11.385	0.035	56446.602	11.312	0.075
56446.652	11.344	0.021	56446.656	11.268	0.078
56446.699	11.309	0.015	56446.703	11.240	0.063
56446.746	11.295	0.029	56446.750	11.233	0.077
56446.797	11.340	0.023	56446.805	11.278	0.080

Note.
[a] MJD = JD — 2400000.5 days.
(This table is available in its entirety in machine-readable form.)

At the end of this process, we obtained a photometric catalog in both IRAC bands for all point sources detected in our field of view. From this catalog, we matched 37 of the 45 RR Lyræ stars with optical photometry derived by Stetson et al. (2014), 26 of them fundamental mode (FU, RRab) pulsators, and 11 pulsating in first overtone (FO, RRc). Of the remaining eight RR Lyræ stars in the cluster, seven are outside of the area mapped in at least one of the two IRAC bands, and one (V64) is a field variable in the background of the cluster, too faint to be detected by IRAC. All M4 RR Lyræ stars are indicated in Figure 1 by squares, with open red and filled blue symbols for FU and FO RR Lyræ stars detected in at least one IRAC band.

The final magnitude of each non-variable star was derived by averaging the value measured in all epochs and in all dithers. For the RR Lyræ variables, we instead preserved the photometry for each epoch, averaging only on the individual dithers, after correcting the photometry in each dither for the warm *Spitzer* location-dependent photometric corrections available at the Spitzer Science Center website.[10] The photometric uncertainty in each epoch is given by the standard deviation of all of the available measurements. A sample of the individual data points for one star, V1, is given in Table 1; all data is available. A few RR Lyræ stars were covered in only one of the five dither positions, and one magnitude measurement was available in each epoch. For these stars (V1, V42, V2, and V29) the photometric uncertainty is instead derived from the repeatability parameter provided by DAOPHOT, which tends to be larger than the photometric error based exclusively on photon and background noise.

3. RR LYRæ LIGHT CURVES AND AVERAGE MAGNITUDES

Our MIR sample of M4 RR Lyræ variables consists of 37 stars, whose locations are shown in Figure 1. Of those, 26 are pulsating in fundamental mode (FU, RRab) and 11 are first overtone pulsators (FO, RRc). Not all sources have complete coverage in the IRAC data set: of the 37 RR Lyræ stars in the

[10] http://irsa.ipac.caltech.edu/data/SPITZER/docs/irac/calibrationfiles/locationcolor/

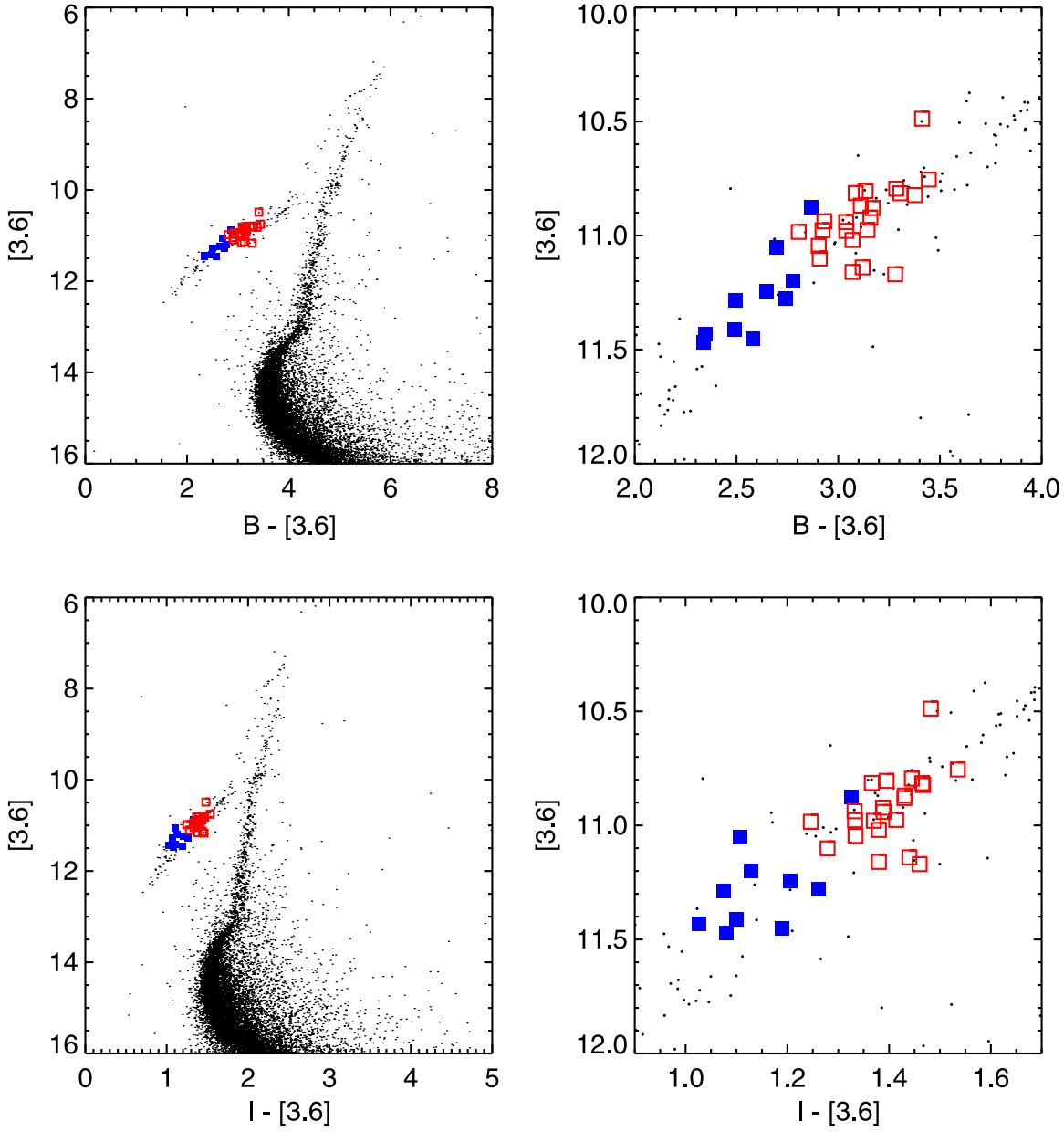

Figure 2. Sample color–magnitude diagrams for all sources detected in the IRAC 3.6 μm band, with B and I photometry from Stetson et al. (2014). Fundamental and first overtone RR Lyræ variables are represented by open red and filled blue squares, respectively. The right panels show a close-up of the horizontal branch.

area mapped by at least one IRAC band, only 28 have photometry at both 3.6 and 4.5 μm, with 6 sources covered only at 3.6 μm and 3 covered only at 4.5 μm. The periods of our RR Lyræ stars range between 0.2275 days (V49) to 0.6240 days (V39), plus a long-period FU RR Lyræ (V52) with a period of 0.8555 days.

Figure 2 shows representative color–magnitude diagrams (CMDs) for M4 based on our MIR and optical photometry, with the IRAC 3.6 μm mag versus the $B - [3.6]$ (top left) and $I - [3.6]$ (bottom left) colors. Note how the high photometric quality of our data allows a well characterized turn-off in all color combinations and a well populated sub-giant, RGB and AGB branch. The FO and FU RR Lyræ stars are represented by filled blue and open red squares, respectively. We see a clear separation of the FO and FU RR Lyræ stars in the horizontal branch of the CMD, with the FO bluer than the FU variables (right panels).

We derived MIR light curves for each RR Lyræ in our catalog by phasing their multiple-epoch photometry based on the epoch of maximum (T_0) and the period derived by Stetson et al. (2014) using the Lomb–Scargle method from the visible data. Sample light curves are shown in Figure 3 for FO variables and 4 for FU variables. The light curves are shown in order of increasing period. Following Madore et al. (2013), for each star, we derived a smoothed light curve using a Gaussian local estimation (GLOESS) algorithm, a method where a second-order polynomial is fit locally and points are weighted by their Gaussian distance from an interpolation point. A full description of the GLOESS method is given in Persson et al. (2004). The mean magnitude for all stars was then determined by integrating the smoothed light curve flux intensity over one period, then converting the result back into a magnitude. The variability amplitude in magnitude was also derived from the smoothed light curve, and the

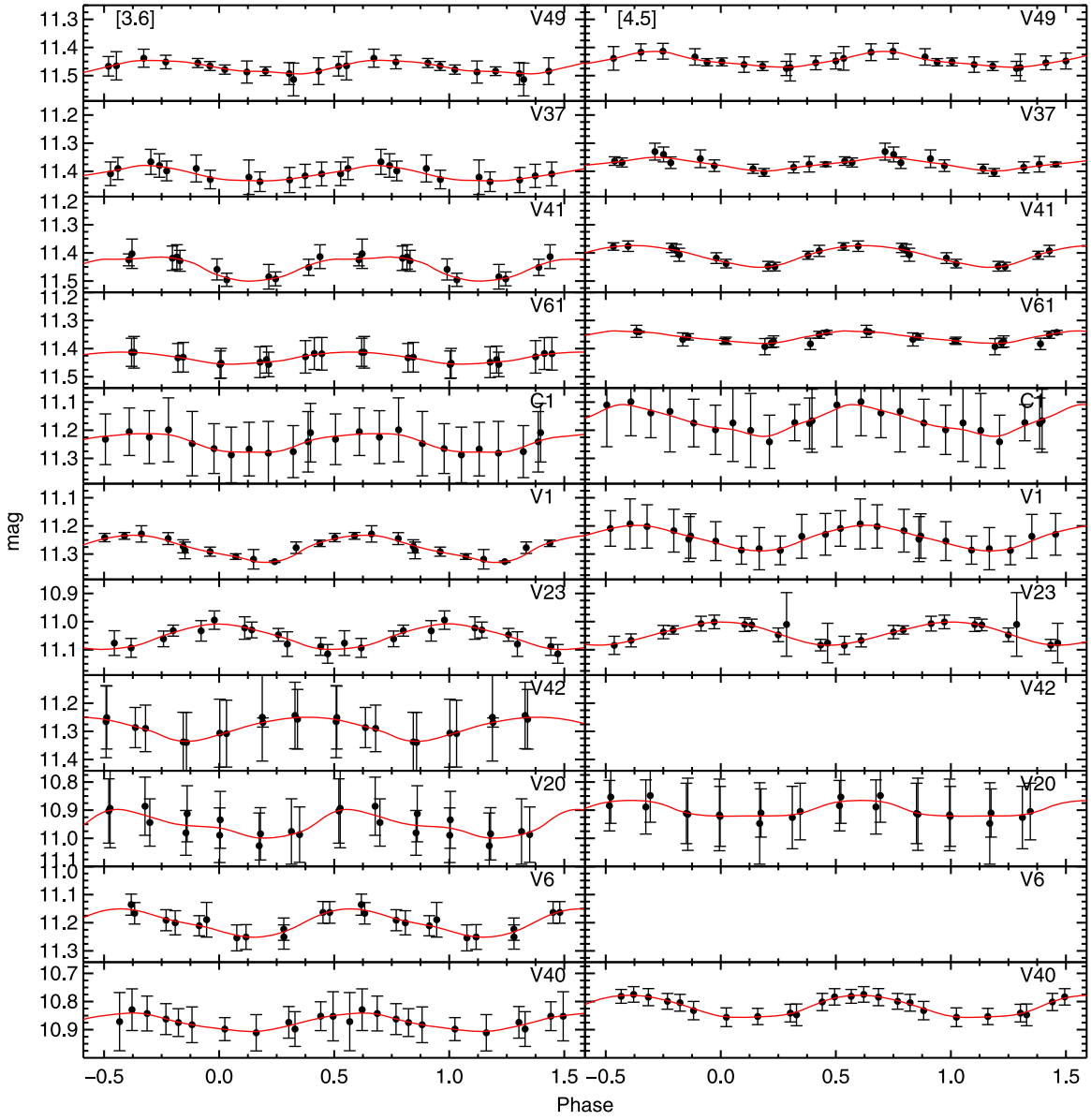

Figure 3. IRAC light curves for all FO RR Lyræ variables in M4. The light curves are arranged from top to bottom in order of increasing period. The left and right panels display the light curves at 3.6 and 4.5 μm. The solid red line is the smoothed light curve generated using a Gaussian local estimator algorithm (see the text for more detail). All light curves cover the same range in magnitude.

uncertainty is calculated using only the data points that lie within the Gaussian window of the maximum and minimum of the smoothed curve.

The uncertainty in the mean magnitude is calculated by the sum in quadrature of photometric uncertainty of each observation $(\sqrt{\Sigma\sigma_i^2}/N)$ and the uncertainty in the fit $(A/(M\sqrt{12}))$ where N is the number of observations, σ_i is the photometric uncertainty, A is the peak-to-peak amplitude, and M is the number of uniformly spaced points (following Scowcroft et al. 2011). The value of M ranges from five to twelve; five (e.g., V41) when our observations cover more than two periods and twelve when our observations cover one complete period (e.g., V5). Some light curves, however, were randomly sampled (e.g., V52, where the observations do not cover a full period), and the uncertainty in the fit is instead $A/\sqrt{12N}$ where N is the total number of observations. Table 2 gives the 3.6 and 4.5 μm IRAC mean magnitudes and amplitudes for the 37 RR Lyræ stars in the IRAC field.

Figure 5 shows the luminosity amplitude versus period (Bailey diagram) for all RR Lyræ stars: filled blue squares for FO and open red squares for FU pulsators. Black crosses indicate FU RR Lyræ stars identified in Stetson et al. (2014) as Blazhko variables (the Blazhko effect is characterized by a conspicuous modulation of amplitude and phase; Blažko 1907). Recent long-term monitoring of Blazhko RR Lyræ by the *Kepler* satellite has provided evidence of not only period-doubling (Szabó et al. 2010) but also the possible occurrence of additional periodicities on a timescale longer than the typical Blazhko period (Chadid et al. 2011; Kolenberg et al. 2011). As expected, the FO and FU RR Lyræ variables are well separated in both period and amplitude, and the amplitude of the FU pulsators show a clear trend of decreasing with period. Figure 6 shows instead the amplitude ratio between optical bands and the IRAC

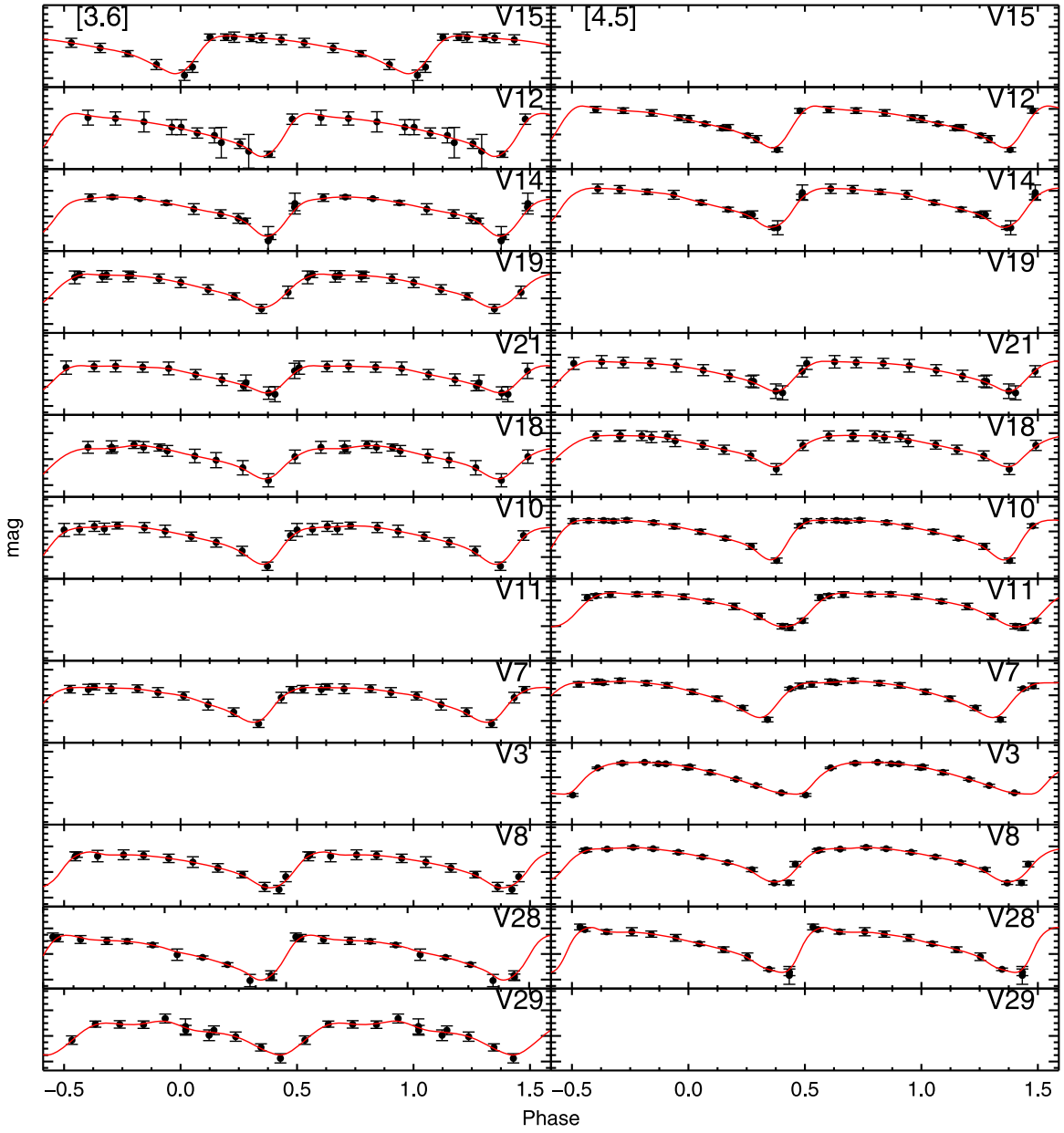

Figure 4. Same as Figure 3, but for all FU pulsators observed by IRAC.

3.6 μm band. The amplitude ratio plot can be used as a diagnostic for blends of stars with different color temperatures. Two FO RR Lyræ stars (V40 and C1) show an unusually high optical-to-MIR ratio, possibly indicative of the presence of a faint optically bright (hot) companion or blend. Another FO RR Lyræ (V49) shows instead an unusually low amplitude ratio, possibly the consequence of having an infrared-bright (cool) companion (or blend). It is also interesting to note that several (four out of seven at 3.6 μm and four out of six at 4.5 μm) of the FU RR Lyræ stars that lie below the general amplitude ratio trend are Blazhko variables, possibly due to these stars being observed at different phases in their amplitude modulation cycle (the optical and MIR data were not acquired simultaneously). If this is the case, the remaining FU RR Lyræ stars in the same amplitude ratio group (V5, V3, and V52) could also be Blazhko stars that were missed by the period studies (or they could be stars with a faint cool companion or blend).

4. MID-IR PL AND PC RELATIONSHIPS

The left panels of Figure 7 show the IRAC PL relation for FO (filled blue squares) and FU (open red squares) RR Lyræ stars in M4. Blazhko variables are indicated by black crosses. The statistical uncertainties of the mean magnitudes are smaller than the size of the plotted symbols, and are not shown. Residuals from the PL relation were used as a diagnostic for blended variables. The central regions of M4 are not particularly dense, and no clear cutoff in radial distance from the center was apparent. Instead, we employed a threshold in sigma to identify candidate blends. Two stars, V20 and V21, in the central regions of the cluster fall outside of the threshold. The variable V20 was over 3σ above the fitted PL relation and, as shown in Figure 4, has a very poor quality light curve. The average magnitude of V21 was more than 5σ above the fitted relation. These stars were not included in the final fit of the PL relations, and are shown in Figure 7 as open circles.

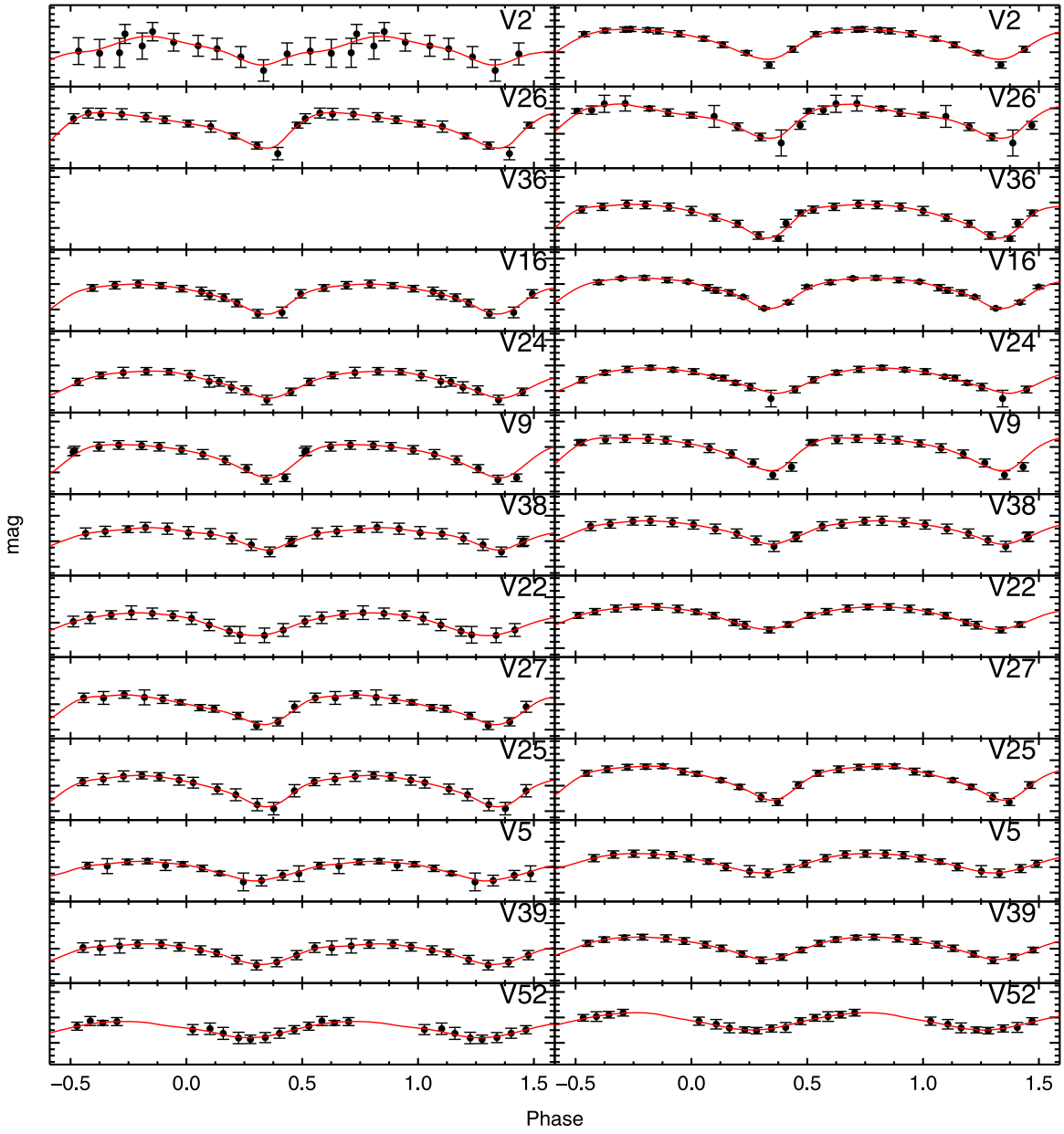

Figure 4. (Continued.)

All average magnitudes are corrected for extinction; albeit MIR extinction corrections are small compared to optical wavelengths, they still cannot be ignored given the high photometric accuracy provided by IRAC. We used the total-to-selective extinctions of $A_{[3.6]}/E(B-V) = 0.203$ and $A_{[4.5]}/E(B-V) = 0.156$ from Monson et al. (2012) and a color excess of $E(B-V) = 0.37 \pm 0.10$ from Hendricks et al. (2012). This results in extinction corrections of 0.075 ± 0.020 and 0.058 ± 0.016 mag at 3.6 and 4.5 μm, respectively.

We calculated the zero point and slope (with their uncertainties and the best-fit standard deviation) for the PL relation using an unweighted least squares fit. An unweighted fit is preferred to avoid biasing by brighter longer period variables, which tend to have smaller photometric uncertainties. The PL relations take the form

$$m = a + b(\log(P) + 0.55) \quad (1)$$

$$m = a + b(\log(P) + 0.26), \quad (2)$$

where $\log(P) = -0.55$ and $\log(P) = -0.26$ are representative of the mean period of the FO and FU variables, respectively. The scatter between the FO and FU PL relations is comparable. Due to the small number of FO variables, we also derived the global PL relations for all RR Lyræ stars (Figure 7, right), having fundamentalized the periods of the FO variables using the relation $\log(P_{\rm FU}) = \log(P_{\rm FO}) + 0.127$ (Iben & Huchra 1971; Rood 1973; Cox et al. 1983). The fundamentalized PL relation takes the form

$$m = a + b(\log(P) + 0.30), \quad (3)$$

where $\log(P) = -0.30$ is representative of the mean fundamentalized period of all RR Lyræ stars in our sample. The zero-point a, slope b, their errors, and the standard deviations for all PL relations are given in Table 3. Note how the secondary

Table 2
Mean IRAC Magnitudes and Amplitudes for the RR Lyræ Stars in M4

ID[a]	α (J2000.0) δ (J2000.0)	Period (days)	$\log(P)$	[3.6] mag	[4.5] mag	Amp $_{[3.6]}$	Amp $_{[4.5]}$	Mode[b]
V1	16 23 13.67 −26 30 53.6	0.28888261	−0.5392786	11.278 ± 0.007	11.244 ± 0.021[c]	0.10 ± 0.01	0.09 ± 0.04	RRc
V2	16 23 16.30 −26 34 46.6	0.5356819	−0.271093	10.976 ± 0.027[c]	10.908 ± 0.010	0.25 ± 0.06	0.28 ± 0.02	RRab*
V3	16 23 19.47 −26 39 57.0	0.50667787	−0.2952681	…	10.982 ± 0.008	…	0.26 ± 0.01	RRab
V5	16 23 21.03 −26 33 05.8	0.62240112	−0.2059296	10.815 ± 0.012	10.758 ± 0.009	0.15 ± 0.04	0.15 ± 0.02	RRab
V6	16 23 25.79 −26 26 16.3	0.3205151	−0.4941515	11.201 ± 0.013	…	0.10 ± 0.02	…	RRc
V7	16 23 25.95 −26 27 41.9	0.49878722	−0.3020847	11.020 ± 0.013	10.977 ± 0.010	0.27 ± 0.02	0.28 ± 0.01	RRab
V8	16 23 26.16 −26 29 41.6	0.50822359	−0.2939452	10.941 ± 0.013	10.896 ± 0.009	0.28 ± 0.02	0.27 ± 0.01	RRab
V9	16 23 26.80 −26 29 48.0	0.57189447	−0.2426841	10.869 ± 0.012	10.814 ± 0.011	0.26 ± 0.02	0.26 ± 0.02	RRab
V10	16 23 29.21 −26 28 54.3	0.49071753	−0.3091684	11.046 ± 0.015	11.002 ± 0.011	0.32 ± 0.03	0.32 ± 0.01	RRab
V11	16 23 29.98 −26 36 24.5	0.49320868	−0.3069693	…	11.029 ± 0.010	…	0.26 ± 0.02	RRab*
V12	16 23 30.82 −26 34 58.9	0.4461098	−0.3505582	11.160 ± 0.023	11.097 ± 0.013	0.34 ± 0.04	0.34 ± 0.01	RRab
V14	16 23 31.29 −26 35 34.5	0.46353111	−0.3339211	11.140 ± 0.017	11.083 ± 0.014	0.32 ± 0.05	0.31 ± 0.04	RRab*
V15	16 23 31.96 −26 24 18.1	0.44366077	−0.352949	11.170 ± 0.014	…	0.31 ± 0.02	…	RRab*
V16	16 23 32.50 −26 30 23.0	0.54254824	−0.2655616	10.880 ± 0.011	10.834 ± 0.008	0.24 ± 0.03	0.24 ± 0.01	RRab
V18	16 23 34.70 −26 31 04.6	0.47879201	−0.3198531	10.980 ± 0.016	10.896 ± 0.014	0.27 ± 0.04	0.25 ± 0.03	RRab
V19	16 23 35.05 −26 25 36.3	0.46781108	−0.3299295	11.101 ± 0.014	…	0.27 ± 0.03	…	RRab
V20	16 23 35.39 −26 32 35.9	0.30941948	−0.5094523	10.953 ± 0.031	10.901 ± 0.031	0.09 ± 0.06	0.06 ± 0.06	RRc
V21	16 23 35.93 −26 31 33.6	0.47200742	−0.3260512	10.752 ± 0.016	10.727 ± 0.016	0.22 ± 0.04	0.24 ± 0.03	RRab
V22	16 23 36.95 −26 30 13.0	0.60306358	−0.2196369	10.795 ± 0.014	10.744 ± 0.009	0.18 ± 0.04	0.18 ± 0.02	RRab*
V23	16 23 37.33 −26 31 56.1	0.29861557	−0.5248876	11.053 ± 0.011	11.043 ± 0.013	0.09 ± 0.02	0.08 ± 0.04	RRc
V24	16 23 38.04 −26 30 41.8	0.54678333	−0.2621847	10.922 ± 0.012	10.900 ± 0.010	0.22 ± 0.02	0.23 ± 0.03	RRab*
V25	16 23 39.42 −26 30 21.3	0.61273479	−0.2127275	10.805 ± 0.013	10.741 ± 0.010	0.26 ± 0.04	0.28 ± 0.02	RRab
V26	16 23 41.65 −26 32 41.1	0.54121739	−0.2666283	10.938 ± 0.013	10.873 ± 0.017	0.32 ± 0.02	0.28 ± 0.04	RRab
V27	16 23 43.17 −26 27 16.3	0.61201829	−0.2132356	10.814 ± 0.012	…	0.24 ± 0.03	…	RRab
V28	16 23 53.60 −26 30 5.30	0.52234107	−0.2820458	10.984 ± 0.013	10.928 ± 0.014	0.36 ± 0.02	0.36 ± 0.02	RRab*
V29	16 23 58.25 −26 21 35.1	0.52248466	−0.2819265	10.977 ± 0.013[c]	…	0.29 ± 0.03	…	RRab*
V36	16 23 19.45 −26 35 49.0	0.54130918	−0.2665546	…	10.900 ± 0.011	…	0.28 ± 0.03	RRab
V37	16 23 31.60 −26 31 30.6	0.24734353	−0.6066994	11.411 ± 0.013	11.376 ± 0.007	0.06 ± 0.03	0.05 ± 0.01	RRc
V38	16 23 32.87 −26 33 03.5	0.57784635	−0.2381876	10.755 ± 0.012	10.708 ± 0.011	0.19 ± 0.03	0.20 ± 0.03	RRab*
V39	16 23 34.67 −26 32 52.1	0.623954	−0.2048474	10.823 ± 0.012	10.779 ± 0.008	0.17 ± 0.03	0.18 ± 0.02	RRab*
V40	16 23 34.59 −26 30 44.2	0.38533005	−0.4141671	10.875 ± 0.020	10.822 ± 0.011	0.07 ± 0.04	0.08 ± 0.02	RRc
V41	16 23 39.50	0.2517418	−0.5990447	11.451 ± 0.011	11.411 ± 0.007	0.09 ± 0.03	0.08 ± 0.01	RRc

Table 2
(Continued)

ID[a]	α (J2000.0) δ (J2000.0)	Period (days)	log(P)	[3.6] mag	[4.5] mag	Amp $_{[3.6]}$	Amp $_{[4.5]}$	Mode[b]
	−26 33 59.8							
V42	16 24 02.00	0.3068549	−0.5130669	11.286 ± 0.032[c]	…	0.09 ± 0.06	…	RRc
	−26 22 13.0							
V49	16 23 45.25	0.22754331	−0.6429359	11.470 ± 0.011	11.448 ± 0.010	0.05 ± 0.03	0.06 ± 0.02	RRc
	−26 31 28.4							
V52	16 23 24.06	0.85549784	−0.0677811	10.488 ± 0.015	10.428 ± 0.015	0.13 ± 0.02	0.14 ± 0.02	RRab
	−26 30 27.8							
V61	16 23 29.76	0.26528645	−0.5762849	11.433 ± 0.015	11.361 ± 0.006	0.04 ± 0.03	0.04 ± 0.01	RRc
	−26 29 50.3							
C1	16 23 36.43	0.2862573	−0.5432434	11.244 ± 0.029	11.168 ± 0.032	0.07 ± 0.06	0.11 ± 0.06	RRc
	−26 30 42.8							

Notes.
[a] The ID given in Clement's catalog, with the exception of C1, newly named in Stetson et al. (2014).
[b] The pulsation mode (RRab = FU, RRc = FO). Candidate Blazhko stars are indicated by an asterisk.
[c] The uncertainty is derived using the repeatability parameter given in DAOPHOT.

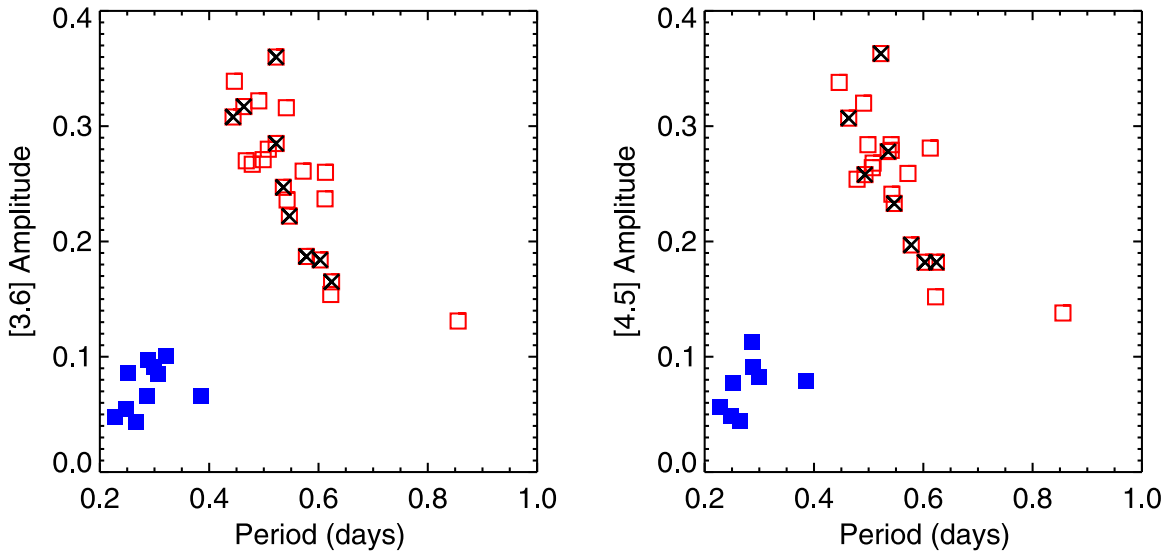

Figure 5. Plot of the IRAC band amplitudes vs. period for RR Lyræ stars in M4 (Bailey diagram). First overtone and fundamental variables are represented by filled blue and open red squares. Candidate Blazhko stars are marked by black crosses.

modulation of the candidate Blazhko variables seem to have no measurable effect on their average magnitudes because they fit well on the PL relation.

Figure 4 in Madore et al. (2013) showed that, using available data, the slope of the RR Lyræ PL relation is a monotonically increasing function of wavelength, and asymptotically approaches a wavelength-independent slope. In Figure 8, we recreate this plot by adding the optical and NIR slopes from Braga et al. (2015), the IRAC MIR slopes calculated above, and the results from Klein et al. (2014). Our data is consistent with the values found by Madore et al. (2013) and Klein et al. (2014) for the *WISE* W1 and W2 bands, and confirm with a high level of accuracy that the slope approaches the value of −2.60 at infrared wavelengths, as predicted by the period–radius relation in Burki & Meylan (1986).

4.1. PC Relationship

Figure 9 shows optical and infrared PC relations for all M4 RR Lyræ variables observed with IRAC (as before, filled blue and open red squares indicate fundamentalized FO and FU). We fit the data with an unweighted least squares procedure; the best-fit parameters are listed in Table 4. The figure clearly shows how the slope of the PC relation becomes more shallow as the distance between the two passbands decreases, as is expected if the color is a temperature effect related to the radius of the pulsator. The $V - K$ PC relation, in particular, has been singled out for being the least affected by temperature uncertainties when deriving RR Lyræ distances with the Baade–Wesselink method (Carney et al. 1992; Cacciari et al. 2000; McNamara & Barnes 2014), as opposed to using the standard $B - V$ color. Our figure shows that PC relationships using MIR colors (and the IRAC 3.6 μm mag in particular) are even more advantageous, thanks to the steeper slope (i.e., $\simeq$1.93 for the $V -$ [3.6] relation versus $\simeq$1.87 in the $V - K$ fit) and slightly smaller dispersion around the best-fit relation.

The last panel in Figure 9 shows the IRAC [3.6] − [4.5] PC relation. In this case, the slope is very shallow (0.046 ± 0.033),

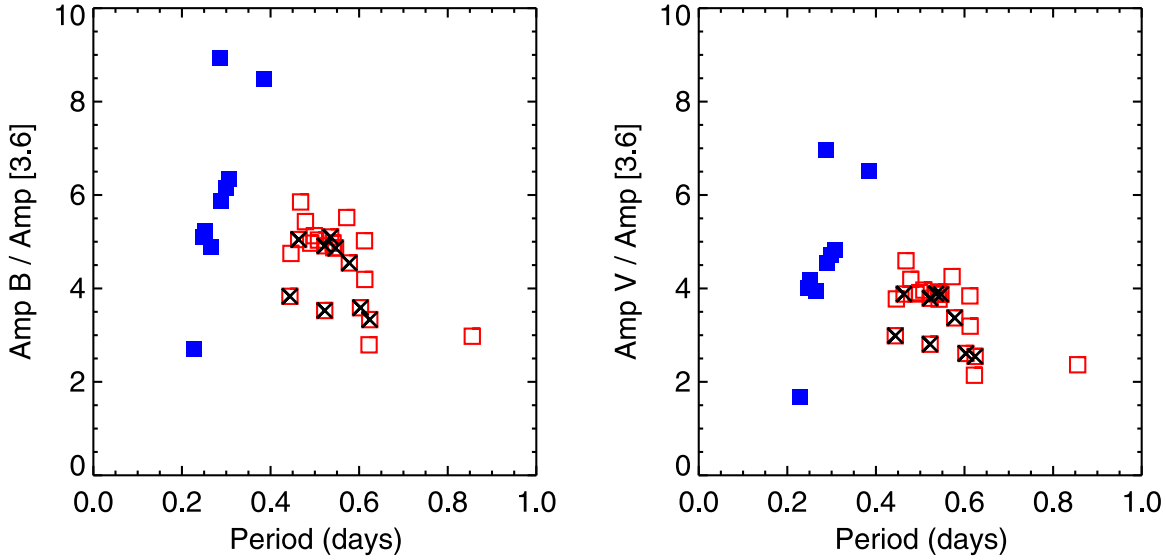

Figure 6. Ratio between the optical and MIR band amplitudes for the first overtone (blue filled squares) and fundamental (red open squares) variables as a function of period. The left plot shows the ratio of the *B* to [3.6] amplitude, while the right plot shows the ratio of *V* band to [3.6] amplitude. Black crosses identify candidate Blazhko variables. The two FO RR Lyræ stars (V40 and C1) that show an unusually high optical to MIR ratio, could possibly indicate the presence of a faint optically bright (hot) companion or blend. The FO RR Lyræ (V49) with an unusually low amplitude ratio, could indicate an infrared-bright (cool) companion (or blend).

consistent with zero within $\sim 1.4\sigma$. The scatter around the best-fit PC relation is also quite large (0.017 mag), three times larger than the uncertainty in the average magnitudes of individual stars. The lack of a significant [3.6] − [4.5] PC relation for RR Lyræ stars suggests that these stars do not develop variable CO molecular absorption in their atmosphere, which is observed in other pulsating stars in the same instability strip (e.g., classical Cepheids). Scowcroft et al. (2011) found a well-defined [3.6] − [4.5] PC relation for LMC Cepheids with $\log P \lesssim 2$. The negative slope of the PC relation and blue colors of these stars is explained by the dissociation and recombination of CO molecules in the IRAC 4.5 μm band, as previously noted by Marengo et al. (2010). This effect is particularly strong in Cepheids with $P > 10$ days and is reflected in a precise phasing of the light and color curve of these stars. Shorter period Cepheids are instead characterized by a flat color curve and red colors. This is further supported by Monson et al. (2012), who found that CO absorption drops off for temperatures greater than 6000 K. Given that these RR Lyræ stars have higher effective temperatures, earlier spectral types, and lower metallicity than Cepheids, it is not surprising that we do not find strong CO effects in the PC relation and color curve. The [3.6]−[4.5] PC relation appears to be flat, even when including Galactic RR Lyræ stars with very different metallicities. Therefore, RR Lyræ observations at 4.5 μm are not limited by strong metallicity effects as Cepheids are, and this band can be successfully used for distance scale measurements with an accuracy similar to that of the 3.6 μm band. The weakness of the 4.5 μm CO band in RR Lyræ stars, however, prevents this feature from being used as a metallicity indicator for this class of variables.

5. MIR PL ZERO POINT CALIBRATION AND M4 DISTANCE MODULUS

The CRRP project relies on establishing RR Lyræ variables as highly accurate indicators for the first rung of the cosmological distance scale, by using their MIR PL relation. The zero point of this relation, however, needs to be calibrated. Efforts in this direction have been made in the recent past by using galactic RR Lyræ stars observed by *WISE* (Madore et al. 2013; Klein et al. 2014), but the accuracy of the calibration has been limited by the uncertainties in the photometry and distance of the calibrators. As mentioned in Section 1, the CRRP project addresses this issue with the observations of 43 Galactic RR Lyræ stars whose geometric parallaxes will be determined better than 2%–3% with *Gaia*, and five bright RR Lyræ stars with parallaxes already determined by Benedict et al. (2011) using the *Hubble Space Telescope* (*HST*) Fine Guidance Sensor (FGS). Ground-based monitoring and spectral observations of the calibrators is ongoing, to ensure the characterization of their pulsation properties and, if required, to allow the calibration of the metallicity dependence of the PL relation.

The observation of a large sample of GGCs (themselves used as distance indicators) as part of the CRRP program provides a separate avenue to test the calibration of RR Lyræ stars and probe for metallicity effects. The distance of M4, in particular, has been the subject of intense analysis, most recently by Braga et al. (2015) by using a theoretical and empirical calibration of the RR Lyræ optical and NIR PL relation for the cluster. The distance modulus derived in this work can be used as an alternative calibration of the MIR PL zero point, as well as to test the effects of metallicity on the zero point derived from the five *HST*/FGS RR Lyræ calibrating stars. A similar approach will be followed for the remaining 30 GCCs in the CRRP program (spanning a wide range in metallicity), for which independent distance moduli will be derived in the optical, NIR, and MIR from their population of RR Lyræ stars.

5.1. Zero Point Calibration Using HST RR Lyræ Stars

As mentioned above, at present there are only five RR Lyræ variables with available geometric parallaxes, i.e., the aforementioned stars observed with *HST*/FGS by Benedict et al. (2011): RR Lyr, UV Oct, SU Dra XZ Cyg (FU pulsators), and RZ Cep (FO). The four FU pulsators are the same stars used by

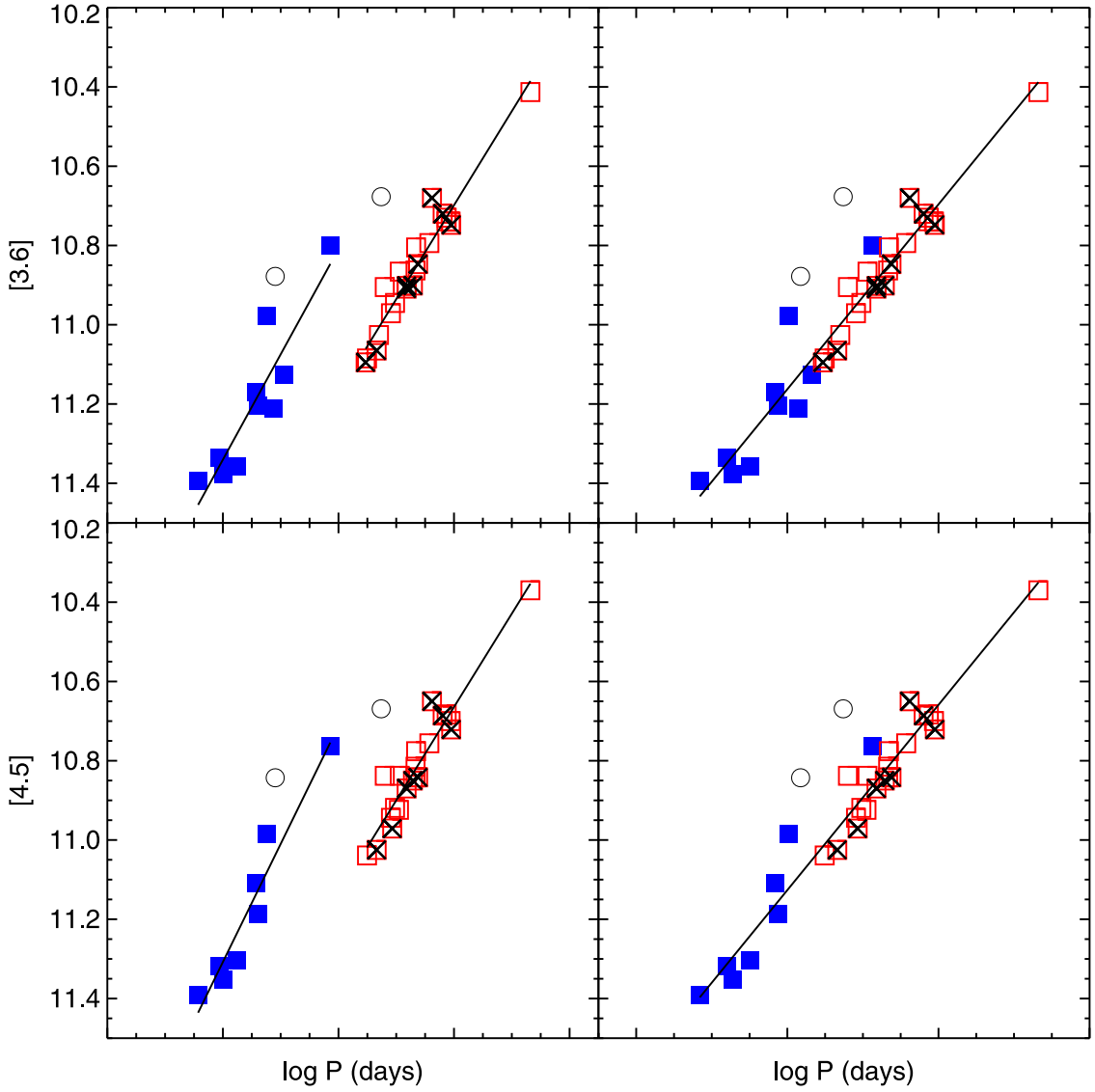

Figure 7. IRAC period–luminosity relations for M4 RR Lyræ stars. (Left) FO (blue filled squares) and FU (red open squares) variables are fit independently (black solid lines). (Right) single fit with fundamentalized FO RR Lyræ stars. All magnitudes are corrected for extinction. Random uncertainties in the average magnitudes of all variables are smaller than the symbols used and are not shown. Candidate Blazhko stars are marked with black crosses. The open circles mark the positions of the two stars (V20 and V21) that were not included in the fit of the PL relation due to blends with nearby sources.

Table 3
Observed MIR Period–Luminosity Relations for RR Lyræ Stars in M4

Band	a^a	b^a	σ	a^b	b^b	σ	a^c	b^c	σ
		FO			FU			FU+FO	
[3.6]	11.207	−2.658	0.079	10.841	−2.370	0.040	10.929	−2.332	0.056
	±0.027	±0.428		±0.009	±0.139		±0.010	±0.106	
[4.5]	11.159	−2.979	0.057	10.806	−2.355	0.045	10.893	−2.336	0.054
	±0.022	±0.337		±0.010	±0.168		±0.010	±0.105	

Notes.
[a] PL parameters of the form $m = a + b(\log(P) + 0.55)$.
[b] PL parameters of the form $m = a + b(\log(P) + 0.26)$.
[c] PL parameters of the form $m = a + b(\log(P) + 0.30)$.

Madore et al. (2013) to calibrate the RR Lyræ PL relation in the *WISE* bands. Even for these stars, however, the uncertainty in their distance modulus is still large (up to 0.25 mag), significantly reducing their effectiveness as calibrators for the distance scale. All five stars have been observed as part of the CRRP program in order to reproduce the Madore et al. (2013) zero point calibration using the IRAC 3.6 and 4.5 μm bandpasses, and with better phase sampling and much smaller

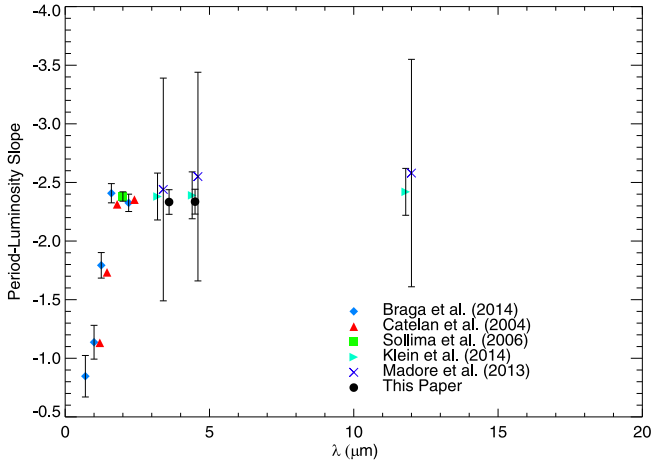

Figure 8. Updated version of Figure 4 from Madore et al. (2013) showing the increase of the slope of the RR Lyræ period–luminosity relation with wavelength. The optical and near-IR slopes are taken from Catelan et al. (2004), Sollima et al. (2006), and Braga et al. (2015). The MIR slopes from Klein et al. (2014) and Madore et al. (2013) are marginally steeper than the values derived in this paper (using IRAC data only), but consistent within their uncertainties. For clarity, results from the same band are offset by 0.2 μm (Catelan +0.2, Sollima −0.2). Error bars are shown for all points, with the exception the theoretical prediction from Catelan et al. (2004).

($\sim$10$\times$ better signal-to-noise ratio) photometric error. Their basic properties (derived from Benedict et al. 2011) are listed in Table 5: their periods range from 0.3086 to 0.6642 days, and their [Fe/H] ranges from −1.43 to −1.83, significantly more metal-poor than M4 itself. A detailed analysis of the calibration of the zero point using these five RR Lyræ stars at multi-wavelengths will be presented in a forthcoming paper.

The mean magnitude of each star was computed as explained in Section 3. Each calibrator was then corrected for extinction, adopting the $E(B-V)$ reddening from Benedict et al. (2011). The extinction corrections were computed using the same $A_{3.6}/E(B-V)$ and $A_{4.5}/E(B-V)$ relations as in Section 3. The absolute mean magnitudes, as well as the parallax, LKH correction (Lutz & Kelker 1973; Hanson 1979), distance moduli, extinction corrections, and apparent mean magnitudes are given in Table 5. Benedict et al. (2011) contains two conflicting results about the parallax to RZ Cep and although the value of 2.12 mas is their preferred solution (G. F. Benedict 2015, private communication), we chose to adopt the 2.54 mas solution with an A_v of 1 (assuming a mean spectral type of A5 (Preston 1959) and $(B-V)_0 = 0.15$) which appears to be more consistent with the new photometric data. The dominating factor in the uncertainty of the absolute mean magnitudes is the uncertainty in their distances.

Based on theoretical NIR PL–metallicity (PLZ) relations, the slope of the RR Lyræ PL relation is expected to be only weakly dependent on metallicity (Braga et al. 2015). Therefore, for this work we elected to adopt the well-constrained slope of the fundamentalized PL relation derived in Section 4, rather than relying on just five Galactic calibrators (having a smaller range in period than the M4 RR Lyræ stars) to simultaneously fit both slope and zero point. Figure 10 shows the resulting PL relation, derived after fundamentalizing the period of RZ Cep. The calibrated PL relations derived using a one parameter fit are given by

$$M_{[3.6]} = -2.332(\pm 0.106)\log(P) - 1.176(\pm 0.080)$$
$$\sigma = 0.095 \quad (4)$$

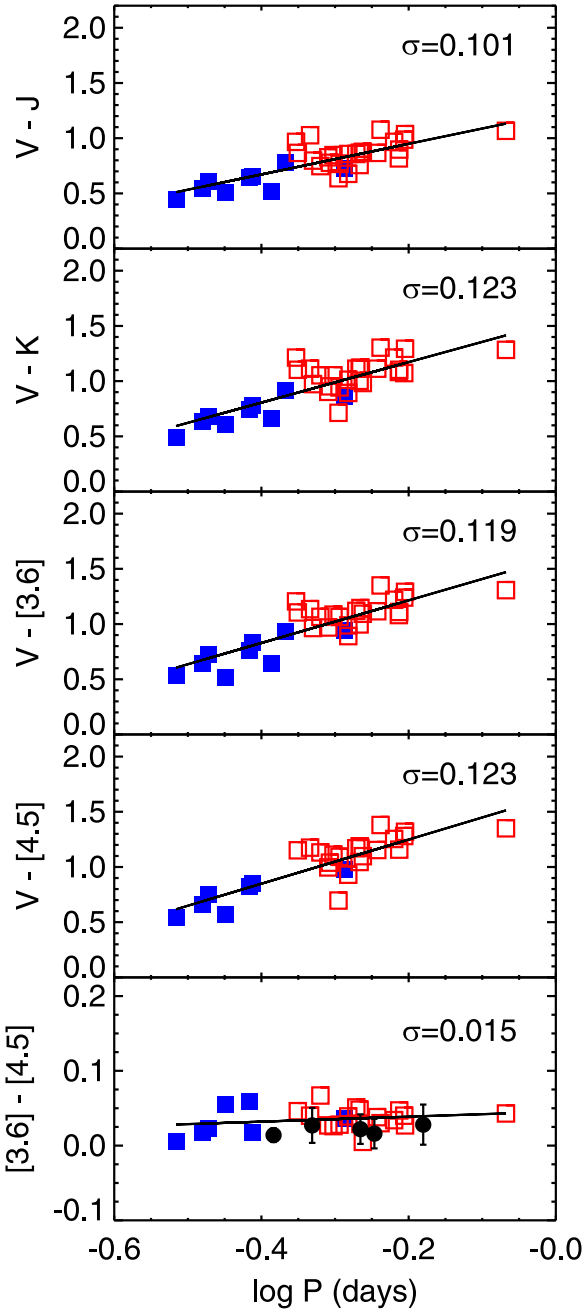

Figure 9. Period–color relationship for the RR Lyræ stars in M4. FO and FU variables observed with IRAC are shown in filled blue and open red squares, respectively, with fundamentalized periods for the FO RR Lyræ. Optical and NIR photometry is derived from Stetson et al. (2014). The solid black line represents the unweighted least squares fit. Five Galactic RR Lyræ stars used for calibration are shown in the bottom panel as black circles (not included in the fit). All magnitudes are corrected for extinction. Note that all panels except the bottom span the same range in magnitude.

$$M_{[4.5]} = -2.336(\pm 0.105)\log(P) - 1.199(\pm 0.080)$$
$$\sigma = 0.095, \quad (5)$$

where the uncertainty in the zero point is calculated by $\sqrt{\sum_i \sigma_i^2}/5$ and σ_i are the uncertainties of the absolute magnitudes for the five calibrator stars used in the fit. The largest factor in the uncertainty of the zero point derived above is due to the uncertainty in the distance modulus of the

Table 4
Fundamentalized Period–Color Relations

Color	a[a]	b[a]	σ
$V-J$	0.808 ± 0.018	1.421 ± 0.192	0.102
$V-K$	0.985 ± 0.021	1.874 ± 0.232	0.123
$V-[3.6]$	1.021 ± 0.021	1.934 ± 0.221	0.117
$V-[4.5]$	1.047 ± 0.023	2.012 ± 0.238	0.121
$[3.6]-[4.5]$	0.034 ± 0.003	0.046 ± 0.033	0.017

Note.
[a] PC parameters of the form color $= a + b(\log(P) + 0.3)$.

calibrators, but it is a factor of three better than the value obtained in Madore et al. (2013) where both the slope and zero point were fit simultaneously and only four stars were used. In both IRAC bands, the slope we obtain is marginally shallower (but still consistent, within the error) than the values published by Klein et al. (2014) and Madore et al. (2013) for the *WISE* W1 and W2 bands. Further improvements on the uncertainty of the zero point will be possible when more accurate parallaxes for all our calibrator RR Lyræ stars are obtained with the *Gaia* mission.

5.2. M4 Distance Modulus

From the zero point calibration of the MIR RR Lyræ PL relation in the previous section, we can derive the true distance modulus of M4:

$$\mu_{[3.6]} = 11.406 \pm 0.010\ (\text{stat}) \pm 0.080\ (\text{syst}) \pm 0.015\ (\text{cal}) \pm 0.020\ (\text{ext}) \quad (6)$$

$$\mu_{[4.5]} = 11.391 \pm 0.010\ (\text{stat}) \pm 0.080\ (\text{syst}) \pm 0.013\ (\text{cal}) \pm 0.016\ (\text{ext}), \quad (7)$$

where we have adopted the M4 PL relation using the fundamentalized period of FO pulsators. The error on the distance modulus comes from four sources. The statistical error is the uncertainty in the zero point of the cluster PL relation and is derived from the least squares fit to the IRAC data. The systematic error is the uncertainty in the calibrated PL zero point, given in the previous section. The calibration error is the dispersion in our photometric zero point calibration to standard IRAC Vega magnitudes, described in Section 2. The extinction error is that derived from the uncertainty due to differential reddening given in Section 4.

The distance modulus we find is slightly larger than expected, based on previous works (11.30 ± 0.05 in Kaluzny et al. 2013; 11.28 ± 0.06 in Hendricks et al. 2012; and 11.35 ± 0.03 ± 0.05 in Braga et al. 2015, this last value derived using RR Lyr itself as a zero point calibrator), but agree within 1σ. If we exclude the systematic error, which will be significantly reduced once high-accuracy geometric parallaxes for a large sample of calibrators become available from *Gaia*, we have an overall uncertainty better than 0.5% in each band. The average distance modulus of the two wavelengths is then

$$\mu = 11.399 \pm 0.007\ (\text{stat}) \pm 0.080\ (\text{syst}) \pm 0.015\ (\text{cal}) \pm 0.020\ (\text{ext}), \quad (8)$$

where the statistical error is reduced by a factor of $\sim\sqrt{2}$ (since by using both bands we take advantage of twice the number of available data points). Note that in this case the overall error is reduced to 1%, small enough to allow for the study of higher order parameters in the RR Lyræ PL relation, first of all, the possible dependence on metallicity, once data from more clusters is analyzed.

Based on the models presented in Braga et al. (2015), while the dependence of the PL slope on metallicity is weak, we do expect a larger effect of [Fe/H] on the PL relation zero point. Therefore, calibrating the PL relation with galactic RR Lyræ stars, all with different metallicities, may induce a significant error. Figure 11 addresses this issue by plotting the residual between the absolute mean magnitude of each calibrator and the value predicted by the PL relation as a function of their

Table 5
IRAC Magnitudes for Galactic RR Lyræ Stars

	RZ Cep	XZ Cyg	UV Oct	RR Lyr	SU Dra
Period	0.308645	0.466579	0.542600263	0.566805	0.660419
[Fe/H]	−1.80 ± 0.2	−1.43 ± 0.2	−1.56 ± 0.11	−1.50 ± 0.13	−1.83 ± 0.2
$E(B-V)$	0.252	0.100	0.090	0.042	0.010
$A_{[3.6]}$	0.051	0.020	0.018	0.009	0.002
$A_{[4.5]}$	0.039	0.016	0.014	0.007	0.002
Parallax (mas)	2.54 ± 0.19[a]	1.67 ± 0.17	1.71 ± 0.10	3.77 ± 0.13	1.42 ± 0.16
LKH correction	−0.05	−0.09	−0.03	−0.02	−0.11
$(m-M)_0$[b]	8.03 ± 0.16	8.98 ± 0.22	8.87 ± 0.13	7.14 ± 0.07	9.35 ± 0.24
[3.6]	7.891 ± 0.007	8.676 ± 0.016	8.200 ± 0.014	6.486 ± 0.014	8.616 ± 0.019
[4.5]	7.865 ± 0.006	8.645 ± 0.017	8.174 ± 0.014	6.468 ± 0.014	8.588 ± 0.019
M [3.6]	−0.190 ± 0.160	−0.324 ± 0.221	−0.688 ± 0.131	−0.663 ± 0.071	−0.736 ± 0.241
M [4.5]	−0.204 ± 0.160	−0.361 ± 0.221	−0.710 ± 0.131	−0.679 ± 0.071	−0.764 ± 0.241

Notes.
[a] Benedict et al. (2011) provide two different parallax values for this star. We adopted the value given in their Section 4.3.2, rather than the number listed in their Table 8, which appears to be inconsistent with the PL relation.
[b] Our distance moduli are slightly different than the values in Table 8 of Benedict et al. (2011) due to typographical errors in that paper.

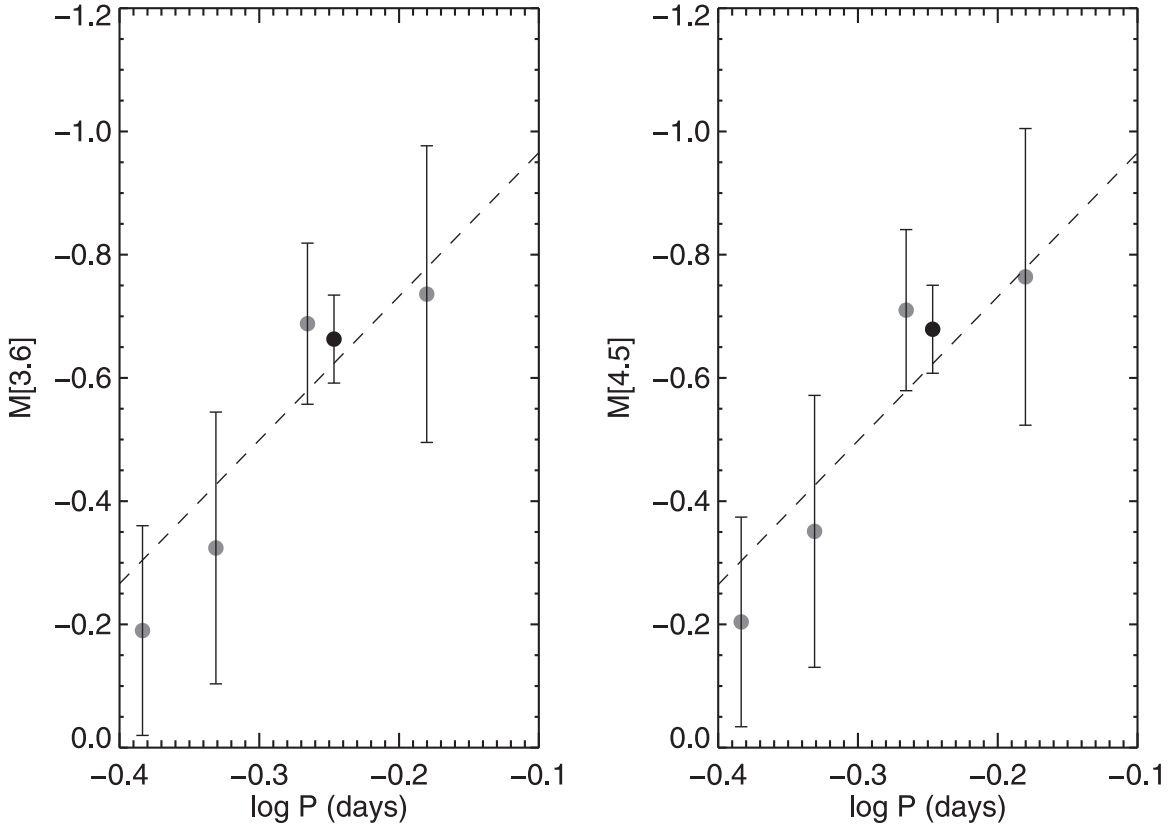

Figure 10. Calibrated IRAC RR Lyræ period–luminosity relation. The filled circles represent the absolute magnitudes of five Galactic RR Lyræ stars. In order of increasing period: RZ Cep, XZ Cyg, UV Oct, RR Lyr (black point), and SU Dra. The period of RZ Cep has been fundamentalized with the same relationship adopted for the M4 FO RR Lyræ stars: $\log P_{FU} = \log P_{FO} + 0.127$. The PL relations are shown by the dashed lines, with a slope determined by the M4 cluster data.

metallicity. The metallicities used in the plot are listed in Table 5, and are the same listed in Benedict et al. (2011, see references therein for the original source of the metallicity measurement), converted from the original (Zinn & West 1984) metallicity scale to the more recent Carretta et al. (2009) scale. For RR Lyr and UV Oct, an extra step was necessary to correct for the different solar abundances used by Kolenberg et al. (2010) when measuring the metallicity of these two stars, with respect to the Carretta et al. (2009). Figure 11 also plots the difference between the M4 distance modulus calculated above for M4, and the value of $11.35 \pm 0.03 \pm 0.05$ derived by Braga et al. (2015) from NIR PL relations calibrated using RR Lyr. Due to the large uncertainties in absolute magnitude and metallicity of the Galactic RR Lyræ stars, no trend is apparent (slope of -0.2 ± 0.3 mag dex^{-1}).

If we adopt the M4 distance modulus value of $11.283 \pm 0.001 \pm 0.018$ derived by Braga et al. (2015) from NIR data and theoretical PLZ relationships for RR Lyræ stars (to avoid the large uncertainty in the calibrator distance that is affecting the zero-point calibration), we obtain the following calibrated RR Lyræ PL relations for the two IRAC bands:

$$M_{[3.6]} = -2.332(\pm 0.106)\log(P) - 1.054(\pm 0.020) \quad (9)$$

$$M_{[4.5]} = -2.336(\pm 0.105)\log(P) - 1.091(\pm 0.020). \quad (10)$$

An in-depth study of the MIR RR Lyræ PL relations based on theoretical models calculated for the IRAC bands will be presented in a forthcoming paper.

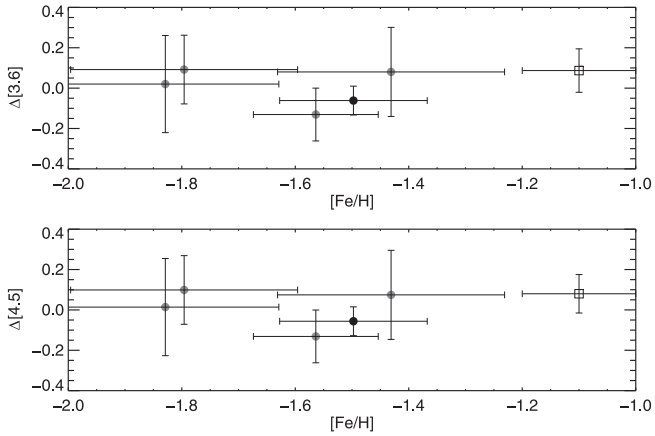

Figure 11. Deviations from the period–luminosity relation as a function of metallicity. Galactic RR Lyræ stars are shown with solid circles (the darker point, with the smallest error bars is RR Lyr) and the average of all stars in M4 is shown as a open square.

6. CONCLUSIONS

We have presented new RR Lyræ MIR PL relations for the nearby globular cluster M4. Accurate IRAC photometry allows us to reduce the error in the PL slope by a factor of at least two from previous works. We have also demonstrated that PL relations in the IRAC bands are consistent with previous calibrations using *WISE* photometry.

We also presented optical and infrared PC relations. The steeper slope and smaller dispersion of the $V - [3.6]$ relation

suggests that it could be preferred over $V - K$ for use in the Baade–Wesselink method. Unlike for Cepheid variables, the [3.6]−[4.5] relation is very shallow, indicating that there is no CO absorption, and therefore little metallicity effect, in the 4.5 μm band. As a result, the 4.5 μm band can be used as a distance indicator.

We calibrated the zero point of the MIR PL relations with five Galactic RR Lyræ stars with known distances. The uncertainty in their distances is the largest source of error, and we will be able to provide a much more precise calibration using upcoming results from the *Gaia* mission. Due to the uncertainty of the available distances to Galactic RR Lyræ stars and the influence of metallicity in the PL relation, we provided a separate PL relation, where the zero point is calibrated using a distance modulus to M4 based on theoretical NIR PLZ relations. Future work will include analyses of the remaining GCCs in the CRRP program in order to provide a comprehensive calibration of the RR Lyræ PL relation. This calibration can then be compared to other distance indicators, such as Type II Cepheids and Delta Scuti variables.

We thank the anonymous referee for providing constructive comments that improved the content of this paper. This work is based [in part] on observations made with the *Spitzer Space Telescope*, which is operated by the Jet Propulsion Laboratory, California Institute of Technology under a contract with NASA. This work was partially supported by PRIN-INAF 2011 "Tracing the formation and evolution of the Galactic halo with VST" (P.I.: M. Marconi) and by PRIN-MIUR (2010LY5N2T) "Chemical and dynamical evolution of the Milky Way and Local Group galaxies" (P.I.: F. Matteucci).

Facilities: Spitzer (IRAC).

REFERENCES

Baade, W. 1944, ApJ, 100, 137
Baade, W. 1957, Obs, 77, 165
Benedict, G. F., McArthur, B. E., Feast, M. W., et al. 2011, AJ, 142, 187
Blažko, S. 1907, AN, 175, 327
Bono, G., Caputo, F., Cassisi, S., Incerpi, R., & Marconi, M. 1997, ApJ, 483, 811
Bono, G., Caputo, F., Castellani, V., Marconi, M., & Storm, J. 2001, MNRAS, 326, 1183
Bono, G., Caputo, F., Castellani, V., et al. 2003, MNRAS, 344, 1097
Bono, G., Stetson, P. B., VandenBerg, D. A., et al. 2010, ApJL, 708, L74
Braga, V. F., Dall'Ora, M., Bono, G., et al. 2015, ApJ, 799, 165
Buonanno, R., Corsi, C. E., Pulone, L., Fusi Pecci, F., & Bellazzini, M. 1998, A&A, 333, 505
Burki, G., & Meylan, G. 1986, A&A, 159, 261
Cacciari, C., & Clementini, G. 2003, in Stellar Candles for the Extragalactic Distance Scale, Vol. 635, ed. D. Alloin & W. Gieren (Berlin: Springer), 105
Cacciari, C., Clementini, G., Castelli, F., & Melandri, F. 2000, in ASP Conf. Series, Vol. 203, The Impact of Large-Scale Surveys on Pulsating Star Research, ed. L. Szabados & D. W. Kurtz (San Francisco, CA: ASP), 176
Caputo, F., Cayrel, R., & Cayrel de Strobel, G. 1983, A&A, 123, 135
Carney, B. W., Storm, J., & Jones, R. V. 1992, ApJ, 386, 663
Carretta, E., Bragaglia, A., Gratton, R., D'Orazi, V., & Lucatello, S. 2009, A&A, 508, 695
Castor, J. I. 1971, ApJ, 166, 109
Catelan, M., Pritzl, B. J., & Smith, H. A. 2004, ApJS, 154, 633
Chaboyer, B., Demarque, P., & Sarajedini, A. 1996, ApJ, 459, 558
Chadid, M., Perini, C., Bono, G., et al. 2011, A&A, 527, A146
Christy, R. F. 1966, ApJ, 144, 108
Cox, J. P. 1963, ApJ, 138, 487
Cox, A. N., Hodson, S. W., & Clancy, S. P. 1983, ApJ, 266, 94
Dambis, A. K., Berdnikov, L. N., Kniazev, A. Y., et al. 2013, MNRAS, 435, 3206
Fazio, G. G., Hora, J. L., Allen, L. E., et al. 2004, ApJS, 154, 10
Fiorentino, G., Stetson, P. B., Monelli, M., et al. 2012, ApJL, 759, L12
Hanson, R. B. 1979, MNRAS, 186, 875
Harris, W. E. 1996, AJ, 112, 1487
Hendricks, B., Stetson, P. B., VandenBerg, D. A., & Dall'Ora, M. 2012, AJ, 144, 25
Hesser, J. E. 1991, Frontiers of Stellar Evolution, Vol. 20 (San Francisco, CA: ASP), 185
Hora, J. L., Marengo, M., Park, R., et al. 2012, Proc. SPIE, 8442, 39
Iben, I., Jr., & Huchra, J. 1971, A&A, 14, 293
Kaluzny, J., Thompson, I. B., Rozyczka, M., et al. 2013, AJ, 145, 43
Klein, C. R., Richards, J. W., Butler, N. R., & Bloom, J. S. 2014, MNRAS, 440, L96
Kolenberg, K., Bryson, S., Szabó, R., et al. 2011, MNRAS, 411, 878
Kolenberg, K., Fossati, L., Shulyak, D., et al. 2010, A&A, 519, AA64
Kollmeier, J. A., Szczygiel, D. M., Burns, C. R., et al. 2013, ApJ, 775, 57
Kunder, A., Stetson, P. B., Cassisi, S., et al. 2013, AJ, 146, 119
Longmore, A. J., Fernley, J. A., & Jameson, R. F. 1986, MNRAS, 220, 279
Lutz, T. E., & Kelker, D. H. 1973, PASP, 85, 573
Madore, B. F., Hoffman, D., Freedman, W. L., et al. 2013, AJ, 117, 135
Majaess, D. J. 2010, JAVSO, 38, 100
Makovoz, D., & Khan, I. 2005, in ASP Conf. Ser. 347, Astronomical Data Analysis Software and Systems XIV, ed. P. L. Shopbell, M. C. Britton, & R. Ebert (San Francisco, CA: ASP), 81
Marconi, M., Coppola, G., Bono, G., et al. 2015, ApJ, in press (arXiv:1505.02531)
Marengo, M., Evans, N. R., Barmby, P., et al. 2010, ApJ, 709, 120
Marín-Franch, A., Aparicio, A., Piotto, G., et al. 2009, ApJ, 694, 1498
McNamara, D. H., & Barnes, J. 2014, AJ, 147, 31
Monson, A. J., Freedman, W. L., Madore, B. F., et al. 2012, ApJ, 759, 146
Oosterhoff, P. T. 1939, Obs, 62, 104
Persson, S. E., Madore, B. F., Krzemiński, W., et al. 2004, AJ, 128, 2239
Plaut, L. 1968, BANS, 2, 293
Preston, G. W. 1959, ApJ, 160, 507
Rood, R. T. 1973, AJ, 184, 815
Sandage, A. 1993, AJ, 106, 687
Sandquist, E. L. 2010, MNRAS, 313, 571
Schuster, M. T., Marengo, M., & Patten, B. M. 2006, Proc. SPIE, 6270, 65
Scowcroft, V., Freedman, W. L., Madore, B. F., et al. 2011, ApJ, 743, 76
Sollima, A., Cacciari, C., & Valenti, E. 2006, MNRAS, 372, 1675
Soszynski, I., Udalski, A., Szymanski, M., et al. 2003, AcA, 53, 93
Stetson, P. B. 1987, PASP, 99, 191
Stetson, P. B. 1994, PASP, 106, 250
Stetson, P. B. 1996, PASP, 108, 851
Stetson, P. B., Braga, V. F., Dall'Ora, M., et al. 2014, PASP, 126, 52
Szabó, R., Kolláth, Z., Molnár, L., et al. 2010, MNRAS, 409, 1244
van den Bergh, S. 1999, A&ARv, 9, 273
VandenBerg, D. A., Brogaard, K., Leaman, R., & Casagrande, L. 2013, ApJ, 775, 134
van Albada, T. S., & Baker, N. 1973, ApJ, 185, 477
Welch, D. L., & Stetson, P. B. 1993, AJ, 105, 1813
Werner, M. W., Roellig, T. L., Low, F. J., et al. 2004, ApJS, 154, 1
Zinn, R., & West, M. J. 1984, ApJS, 55, 45